Molecular Therapy
Nucleic Acids
Original Article

miRNA-199b-5p suppresses of oral squamous cell carcinoma by targeting apical-basolateral polarity via Scribble/Lgl

Shihyun Kim,[1] Suyeon Park,[1] Yong-Jae Kim,[2] Jeongeun Hyun,[2,3] and Jongho Choi[1]

[1]Department of Oral Pathology, College of Dentistry, Gangneung-Wonju National University, Gangneung-si, Gangwon-do 25457, Republic of Korea; [2]Department of Nanobiomedical Science & BK21 NBM Global Research Center for Regenerative Medicine, Dankook University, Cheonan-si, Chungcheongnam-do 31116, Republic of Korea; [3]Department of Biomedical Sciences & Biosystem, College of Bio-convergence, Dankook University, Cheonan 311166, Republic of Korea

In epithelial cells, Scribble forms cell-cell junctions and contributes to cell morphology and homeostasis by regulating apical-basolateral polarity in mammals and functions as a tumor suppressor in many carcinomas. The initial diagnosis of oral squamous cell carcinoma is important, and its prognosis is poor when accompanied by metastasis. However, research on the mechanisms of oral squamous cell carcinoma metastasis is insufficient. Herein, we showed that Scribble regulates the apical-basolateral polarity of oral squamous cell carcinoma by regulating lethal giant larvae 1, Scribble module and E-cadherin, the adhesion junction. The expression of lethal giant larvae 1 and E-cadherin decreased when the expression of Scribble was knocked down and their localization was completely disrupted in both the oral squamous cell carcinoma cell line and *in vivo* model. In particular, the Scribble was involved in oral squamous cell carcinoma metastasis via hsa-miR-199b-5p, which is a microenvironmental factor of hypoxia. The disruption of Scribble localization under hypoxic conditions, but its localization was maintained in miR-199b-5p oral squamous cell carcinoma cell lines and *in vivo*. These results suggest that Scribble functions as a tumor suppressor marker mediated by miR-199b-5p in oral squamous cell carcinoma.

INTRODUCTION

Oral cancer is the most common cancer worldwide and encompasses all tumors that develop within the oral cavity, including the tongue, mouth, floor, and palate.[1] According to the 2019 Global Burden of Disease study, approximately 400,000 new cases occur every year, and 200,000 patients (50%) have oral cancer mortality worldwide.[2] Oral squamous cell carcinoma (OSCC) accounts for more than 90% of all oral cancers, and its incidence is increasing in Asian countries.[3,4] One of the key characteristics of OSCC is its propensity for local invasion and lymph node metastasis; the 5-year survival rate of patients with metastasis is less than 50%.[5,6] Currently, there is no specific clinical treatment available for metastasis[7] because the process of tumor metastasis involves dynamic changes in the morphology of tumor cells, driven by intracellular signaling and extracellular communication with the complex tumor microenvironment (TME).[8–10] Therefore, understanding the mechanisms of OSCC metastasis by diverse TME facilitates the identification of treatment and prognostic factors and is critical for improving OSCC treatment.[7]

Cell polarity plays a pivotal role as an intracellular factor in the malignant progression of OSCC and other epithelial cell tumors.[7,11,12] Scribbles, in conjunction with discs large (Dlg) and lethal giant larvae (Lgl), play a critical role in establishing and maintaining the apical-basolateral polarity (ABP) of cells, thereby influencing both the normal epithelial cell structure and the dynamics of tumor growth.[13,14] In *Drosophila*, mutations in the Scribble protein have been shown to disrupt cell polarity and promote the development of neoplastic tumors, and metastasis cooperates with the Notch oncogene.[15] In cancer studies, Scribble upregulation has been observed in diverse cancer types, contributing to cancer cell proliferation and metastasis.[14,16] However, the expression of Scribble is not uniform in diverse tumor types, and its functional roles remain controversial.[17] Edamana et al. showed that Scribble is downregulated in breast tumor tissues, and its expression affects tumor size and metastasis differently.[18] Furthermore, in lung cancer, inhibition of Scribble expression has been shown to suppress apoptosis through Nox2/ROS signaling, promoting tumor growth.[19] However, the impact of Scribbles on OSCC progression and its underlying mechanisms remain unexplored.

Hypoxia is the most common feature of solid tumors and a pivotal TME that determines the behavior of tumor cells.[20] In tumor cells exposed to hypoxic conditions, epigenetic changes can affect cellular reprogramming,[21] which is initiated by the stabilization of hypoxia-inducible factor-1 (HIF-1), triggering molecular events, such as epithelial-mesenchymal transition (EMT).[22–24] Another epigenetic change under hypoxic conditions was recently identified: hypoxia-inducible microRNA

Received 5 June 2024; accepted 16 October 2024;
https://doi.org/10.1016/j.omtn.2024.102363.

Correspondence: Jongho Choi, Department of Oral Pathology, College of Dentistry, Gangneung-Wonju National University, Gangneung-si, Gangwon-do 25457, Republic of Korea.
E-mail: jhchoi@gwnu.ac.kr

Published by Elsevier Inc. on behalf of The American Society of Gene and Cell Therapy.
This is an open access article under the CC BY-NC-ND license (http://creativecommons.org/licenses/by-nc-nd/4.0/).

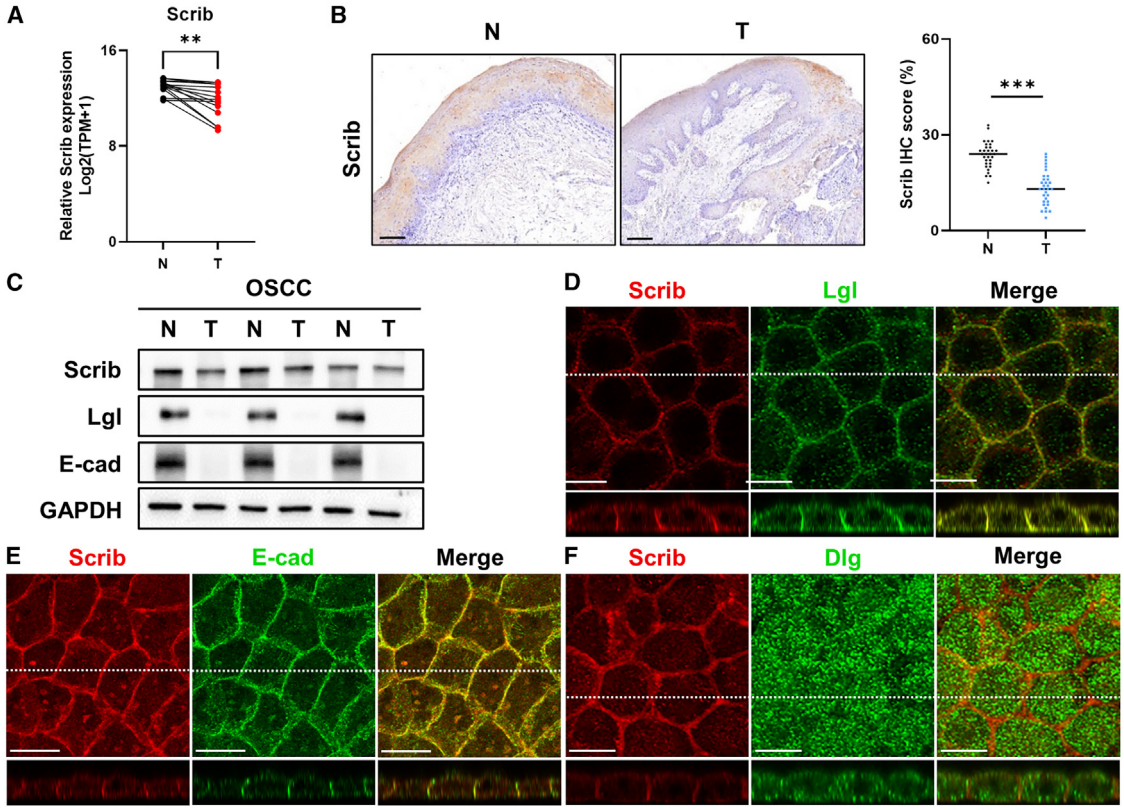

Figure 1. Scribble is downregulated in patients with OSCC and human OSCC cell lines

(A) Analysis of Scribble mRNA expression levels in adjacent non-tumorous tissues and tumor of OSCC (GEO-GSE37991). (B) Representative images of immunohistochemistry staining of OSCC and tissues from OSCC without or with lymph node metastasis. Scribble expression scores are shown in the dot plot. Normal and different grades of OSCC tissues were matched and compared using a paired Student's t test. $n = 33$. Original histology magnification, ×20. Scale bar, 100 μm. (C) Western blot analysis of Scribble, E-cadherin, and Lgl1 in protein extracts from human normal squamous cell and OSCC cells. GAPDH was used for loading control. (D–F) Immunofluorescence for Scribble (red) with E-cadherin, Lgl1 and Dlg1 (green) in the SCC-9 cell line. The z stacks were analyzed in three confocal slices. Original histology magnification, ×60. Scale bar, 20 μm. Statistical significance was assessed by Student's t test. ***$p < 0.001$, **$p < 0.01$.

(HRM), a short non-coding RNA.[25] In general, 6% of these microRNAs (miRNAs) contain putative hypoxia response elements in their promoters, which are present in the promoters of hypoxia-inducible genes.[26,27] However, even if miRNAs interact directly with HIF-1, their effects on tumor progression are not consistently observed.[25] In addition, while studies have explored miRNAs linked to alterations in the morphology of cancer cells in different cancer types,[28–31] there remains a need for more extensive research focused on HRMs that collaborate with HIF-1 and a deeper understanding of their precise mechanisms.

In the present study, we have provided evidence that Scribble serves as a prominent tumor suppressor, highlighting the inverse relationship between HIF-1α and Scribble in both *in vivo* and *in vitro* experiments of OSCC under hypoxia exposure. Hypoxia is a prominent factor in solid TME and is closely associated with alterations in ABP in OSCC. Our findings unveiled the miRNA-199b-5p/HIF-1α axis as a key regulatory pathway induced by hypoxia, playing a pivotal role in mediating hypoxia-induced ABP changes through interaction with Scribble. Furthermore, additional research has demonstrated that the miRNA-199b-5p/HIF-1α axis contributes to essential biological outcomes, including the growth and metastasis of OSCC.

RESULTS

Scribble forms a junction with Lgl1 in the OSCC cell line

To examine the expression of Scribble in OSCC, we initially analyzed Scribble expression in OSCC using a public database. The mRNA expression of Scribble was significantly lower in OSCC tissues than in normal tissues (Figure 1A). Immunohistochemistry (IHC) and western blotting analyses showed that Scribble protein levels were downregulated in OSCC tissues compared with adjacent normal tissues (Figures 1B and 1C). In addition, Scribble expression in OSCC tissues correlated with tumor stage and lymph node metastasis (Table S1). In general, Scribble is a constituent of ABP complexes, and together with Dlg and Lgl, it serves as a pivotal protein in maintaining the integrity of adherens junctions (AJs) at the cell-cell contact area.[32,33] Therefore, to verify the correlation among the three proteins in OSCC cell lines, we first confirmed their localization. Our results showed that Scribble co-localized with E-cadherin (Figure 1D), and

both proteins were distributed within the AJs at the cell-cell region in the SCC-9 cell lines (Figure 1D, z stack image). Furthermore, co-localization of Scribble and Lgl1 was detected (Figure 1E), and they displayed localized expression within the AJs in SCC-9 cell lines (Figure 1E, z stack image). However, Scribble was mislocalized with Dlg1, and the expression of Dlg1 was detected within the cytoplasm (Figure 1F). These results suggest that the expression of Scribble is negatively associated with OSCC progression and cooperates with Lgl1 in AJs, but not Dlg1.

Scribble cooperatively regulates the metastatic and proliferative properties of OSCC with Lgl1

To provide direct evidence that Scribble regulates the expression and localization of AJs in cell-cell interactions, we knocked down Scribble using small interfering RNA (siRNA) in SCC-9 and HSC-2 cells, which are known for their aggressive capacity in previous studies.[34] Following the knockdown of Scribble, the expression of Lgl1 and E-cadherin was remarkably reduced compared with that in the control (Figure 2A). Our co-immunoprecipitation studies showed that the Scribble protein acts as a binding partner for Lgl1, and this interaction was disrupted after Scribble knockdown in both cell lines (Figure 2B). Furthermore, confocal microscopy revealed that after Scribble knockdown, the expression of Lgl1 and E-cadherin disappeared in the cell-cell contact area (Figures 2C, 2D, S1A, and S1B), disrupting the AJs compared with control cells (Figure 2D, z stack image). We hypothesized that the disruption of AJs by Scribble reduction may alter the metastatic properties of OSCC cells. To conclude, the migration and invasion abilities of SCC-9 and HSC-2 cell lines were compared with those of control cell lines after Scribble knockdown. Our results demonstrated that in both SCC-9 and HSC-2 cell lines, the number of cells migrating and invading from the upper insert to the lower insert was significantly reduced following treatment with siRNA-Scribble, in comparison with the control cell lines (Figures 2E and 2F). In addition, EdU assay results showed that the proliferation capacity of SCC-9 and HSC-2 cell lines, following knockdown of Scribble, was significantly reduced compared with that of control cells (Figures 2G and 2H). Taken together, our results suggest that the Lgl1 is mediated by Scribble, may play a crucial role in regulating ABP in OSCC cells, and that these alterations, in turn, influence the metastatic and proliferative properties of OSCC cells.

Hypoxia modulates the localization of ABP in the OSCC cell lines via Scrib/Lgl1

Cellular barriers such as tight junctions in carcinoma cells collapse in response to hypoxic conditions, which are mediated by HIF-1α expression.[35] Hence, to explore whether OSCC cells cultured under hypoxic conditions induce modifications in ABP mediated by the Scribble protein, we investigated the co-localization between Scribble and E-cadherin or Scribble and Lgl1 in OSCC cell lines under hypoxic conditions. Immunofluorescence analysis revealed that the localization of Scribble at ABP in OSCC cells was attenuated by hypoxic incubation (Figures 3A and S2A), and the co-localization of Scribble-Lgl1 was disrupted under hypoxic conditions compared with normoxic conditions (Figures 3B and S2B). Furthermore, the expression of Scribble and Lgl1 was decreased in both SCC-9 and HSC-2 cell lines, whereas alterations in E-cadherin expression were rare in the HSC-2 cell lines after hypoxic conditions (Figure 3C). In our previous studies, we screened for miRNAs that were negatively expressed in OSCC cultured under hypoxia and targeted HIF-1α.[36] Among these miRNAs, miRNA-199b-5p, which exclusively targets HIF-1α without affecting Scribble expression, was identified using the public algorithm set (Figures S3A and S3B). The mRNA expression of miRNA-199b-5p was significantly reduced in SCC-9 and HSC-2 cells under hypoxic conditions compared with that under normoxic conditions (Figure 3D). Luciferase activity assay showed that miRNA-199b-5p downregulated HIF-1α by binding to the predicted target sites in the 3′-UTR of HIF-1α (Figure 3E). Our findings indicate that hypoxia disrupts ABP localization in OSCC cells via Scribble expression.

miRNA-199b-5p suppresses the metastatic and proliferative properties of OSCC via scrib/Lgl1

To investigate the miR-199b-5p effects on OSCC, we confirmed in the mRNA public database that the expression of miR-199b-5p was significantly decreased in OSCC tissues from paired OSCC tumors and adjacent normal tissues (Figure S3C). In addition, the mRNA of miR-199b-5p expression was significantly downregulated in OSCC tissues compared with normal tissues (Figure S3D). Next, to verify if miRNA-199b-5p impacts the ABP, we examined the expression of HIF-1α, Scribble, and Lgl1 using western blotting after miRNA-199b-5p delivery. In both SCC-9 and HSC-2 cell lines, treatment with the miRNA-199b-5p mimic decreased HIF-1α expression, while the expression of Scribble and Lgl1 increased compared with the control group. However, differences in E-cadherin expression remain rare in HSC-2 cells (Figure 4A). Furthermore, in SCC-9 and HSC-2 cell lines treated with the miRNA-199b-5p mimic, the Scribble and Lgl1 proteins exhibited stronger binding than in the control group (Figure 4B). Immunofluorescence results revealed that the co-localization of Scribble and E-cadherin at the ABP was noticeable after treatment with miRNA-199b-5p (Figures 4C and S4A). This finding indicates that miRNA-199b-5p, which targets HIF-1α, indirectly affects the arrangement of the ABP in OSCC cells by modulating the interaction between Scribble and Lgl1 (Figures 4D and S4B). The Boyden chamber assay showed that migration and invasion abilities were significantly decreased in SCC-9 and HSC-2 cells treated with miRNA-199b-5p compared with those in control cells (Figures 4E and 4F). In addition, the proliferation capacity of SCC-9 and HSC-2 cell lines following treatment with the miRNA-199b-5p mimic was significantly reduced comparing with that of control cells (Figures 4G and 4H). These findings suggest that the HIF-1α target miRNA-199b-5p enhances the stability of the ABP in OSCC cells, thereby suppressing their metastatic properties.

Scribble deficiency promotes the tumor growth and metastasis of OSCC *in vivo*

To explore whether Scribble-induced events *in vitro* were also observed *in vivo*, SCC-9 cells transfected with siRNA-negative control

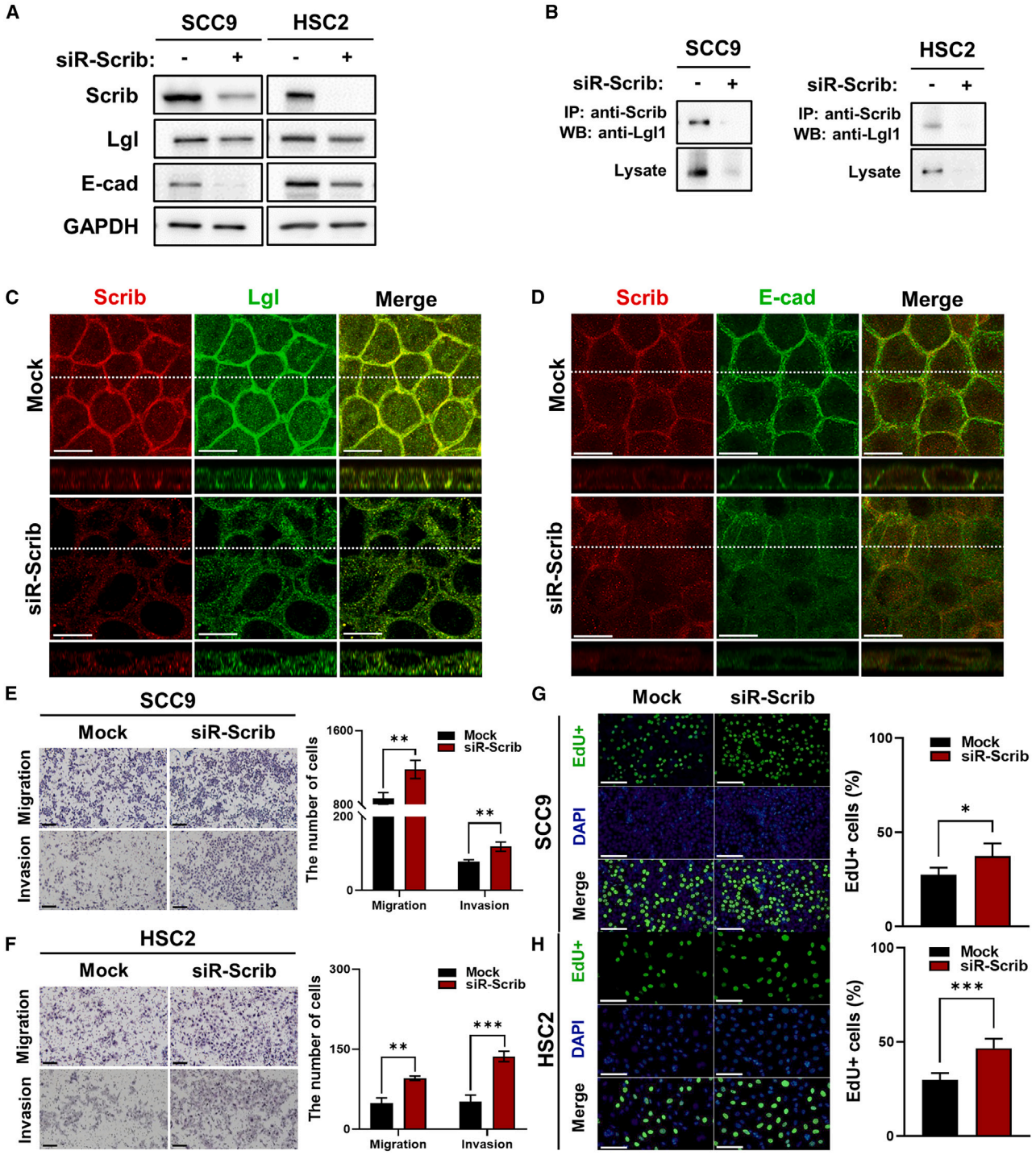

Figure 2. Scribble inhibition induces cell mobility and proliferation in OSCC cell lines

(A) Western blot analysis of Scribble, Lgl1 and E-cadherin in protein extracts from OSCC cell lines. GAPDH was used for loading control. (B) Immunoprecipitation of Lgl1 for the knockdown of Scribble in protein extracts from human OSCC cell lines. (C and D) Representative images of immunofluorescence for Scribble (red) with E-cadherin and Lgl1 (green) by inhibition of Scribble in the SCC-9 cell line. The z stacks were analyzed in three confocal slices. Original histology magnification, ×60. Scale bar, 20 μm. (E and F) Representative images (left) and numbers (right) of migrated and invaded cells by inhibition of Scribble in SCC-9 and HSC-2 cell lines. Original histology magnification, ×20. Scale bar, 100 μm. (G and H) Representative images (left) and numbers (right) of EdU-positive cells (green) for proliferation analysis by inhibiting Scribble. The nuclei were stained with DAPI (blue). Original histology magnification, ×20. Scale bar, 20 μm. Statistical significance was assessed by Student's t test. ***$p < 0.001$, **$p < 0.01$, *$p < 0.05$.

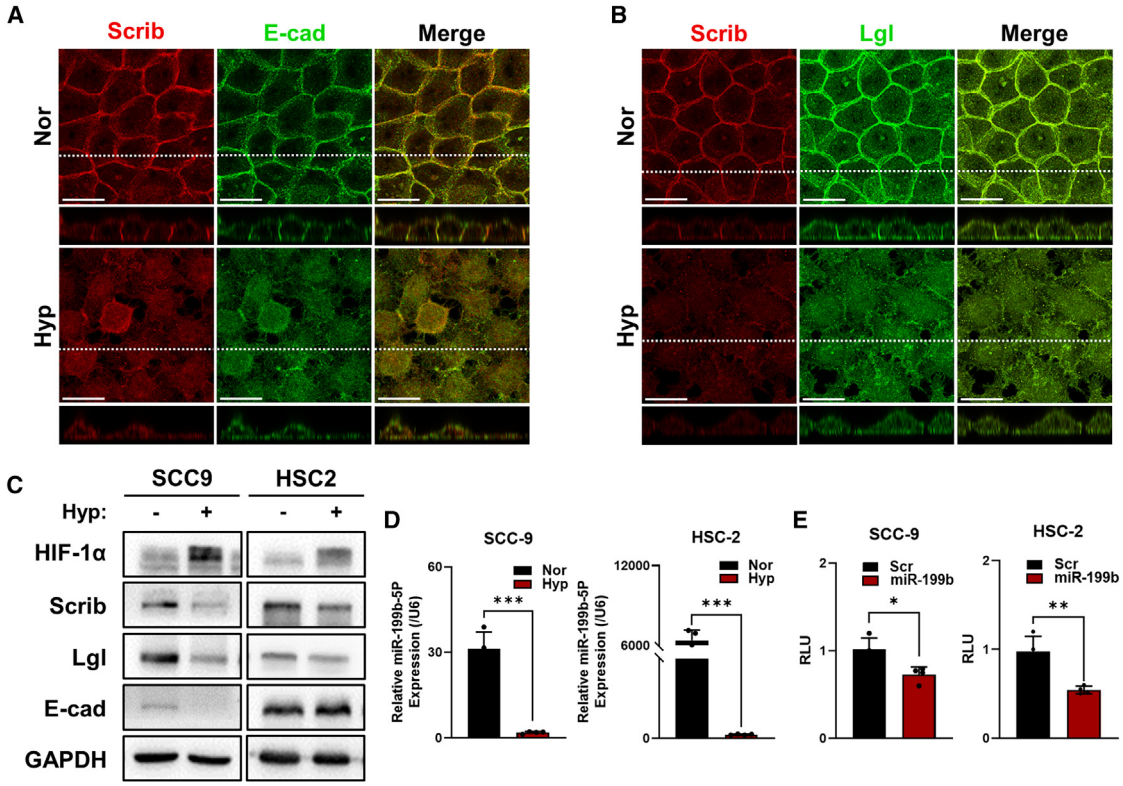

Figure 3. Hypoxia suppresses Scribble, and miR-199b-5p binds directly to HIF-1α

(A and B) Immunofluorescence for Scribble with E-cadherin and Lgl1 in SCC-9 cells under hypoxic condition. The z stacks were analyzed in three confocal slices. Original histology magnification, ×60. Scale bar, 20 μm. (C) Western blot analysis of HIF-1α, Scribble, E-cadherin, and Lgl1 in protein extracts from OSCC cell lines under hypoxic condition. GAPDH was used for loading control. (D) Relative mRNA expression level of miRNA-199b using real-time PCR in OSCC cell lines under hypoxic condition. (E) Luciferase activity of miR-199b and HIF-1α was performed using a Dual-Glo Luciferase assay in OSCC cell lines under hypoxic condition. Relative luciferase activity (RLU) is shown as mean ± SEM compared with four experimental repetitions. Statistical significance was assessed by Student's t test. ***$p < 0.001$, **$p < 0.01$, *$p < 0.05$.

or siRNA-Scribble were subcutaneously injected into BALB/c nude mice. Three weeks after cell injection, the tumor size treated with siRNA-Scribble increased noticeably compared with that in the control group (Figure 5A, left). Furthermore, tumor weight was significantly increased in the siRNA-Scribble-treated tumor compared with that in the control group (Figure 5A, right). qRT-PCR analysis revealed that the mRNA expression of Lgl1 and E-cadherin was significantly decreased in tumor tissues with Scribble knockdown compared with control tumor tissues, and the reduction was dependent on Scribble expression (Figures 5B–5D). Subsequently, to examine whether alterations in AJs depend on Scribble in tumor tissues, we assessed their localization. In the tumor tissues of the control group, co-localization of Scribble and E-cadherin was observed in regions of cell-cell contact (Figure 5E, upper panel). However, in the tumor tissues of the siRNA-Scribble group, co-localization in cell-cell contact regions was not observed (Figure 5E, lower panel). Additionally, the expression of Lgl1 shifted from the cell-cell contact region to the cytoplasm after Scribble knockdown, in contrast to the control group (Figure 5F). To assess the impact of the Scribble expression-dependent redistribution of ABP on OSCC metastasis, SCC-9 cells were intravenously injected, and the hAlu repeat sequence in the lung was analyzed. Analysis of Alu sequences is the preferred method for assessing the biodistribution of injected cancer cells in xenogeneic animal models.[37] The expression of Alu sequences was notably higher in the lungs of the siRNA-Scribble group than in the lungs of the control group (Figure 5G). Histopathological analysis showed that metastasis of OSCC cells inhibited Scribble expression in the lungs more frequently than in the control group (Figure 5H, left), and the size of tumor colonies also significantly increased (Figure 5H, right). These findings suggest that the loss of Scribble disrupts the apical-basal junction in OSCC cells, resulting in OSCC tumor growth and metastasis.

miR-199b-5p inhibits the growth and metastasis of OSCC *in vivo*

Since our *in vitro* experiments demonstrated that miRNA-199b-5p inhibited the proliferative and metastatic properties of OSCC cell lines, we further investigated whether miRNA-199b-5p could inhibit tumor growth and metastasis *in vivo*. The size of the subcutaneous tumors injected with miRNA-199b-5p was significantly reduced compared with that in the control group (Figure 6A, left). Furthermore, the tumor weight in the miRNA-199b-5p treatment group was remarkably lower than that in the control group (Figure 6A,

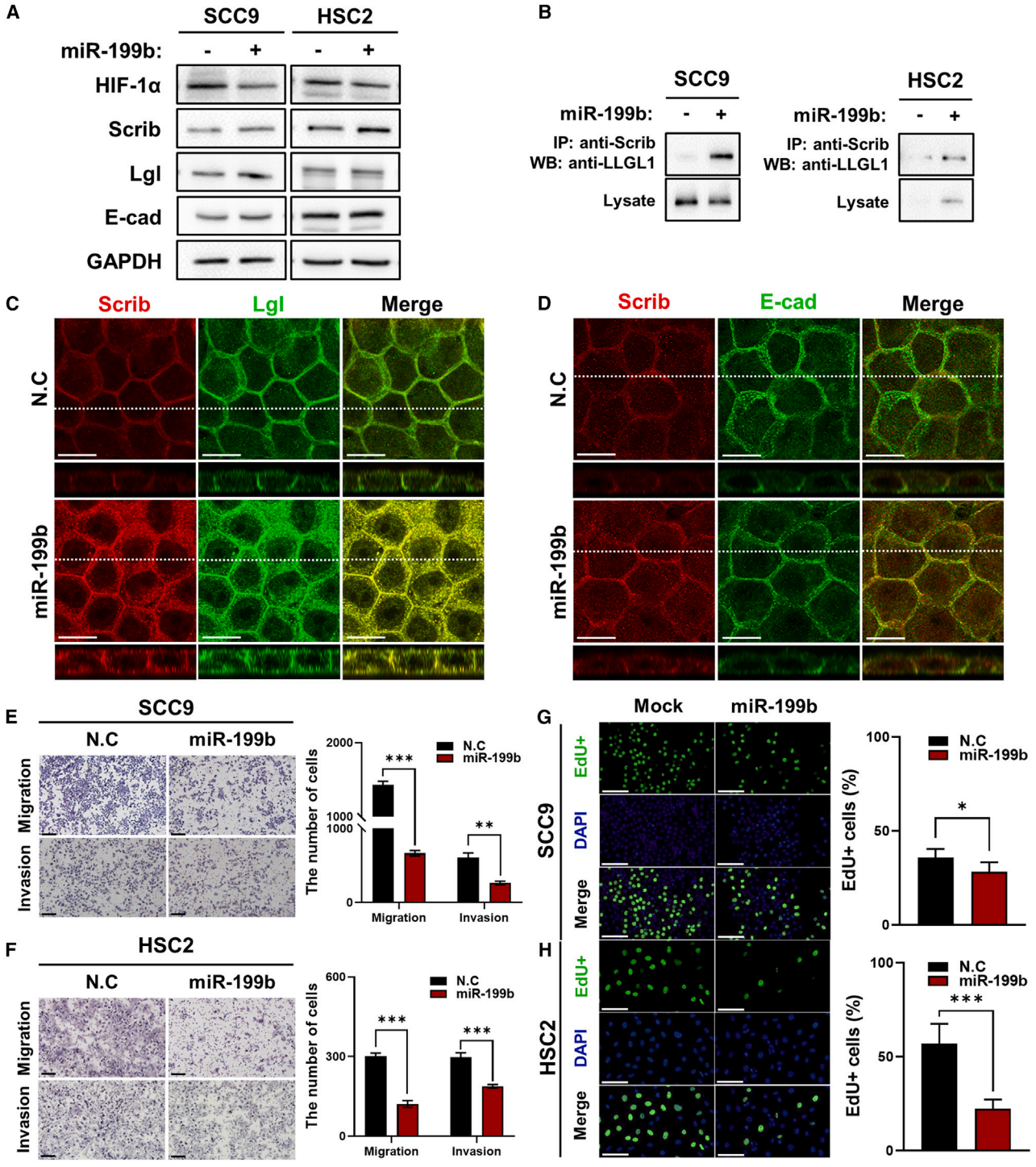

Figure 4. miR-199b-3p reduces cell mobility and proliferation in OSCC cell lines

(A) Western blot analysis of Scribble, E-cadherin, and Lgl1 in protein extracts from OSCC cell lines. GAPDH was used for loading control. (B) Immunoprecipitation of Lgl1 transfected by miR-199b in protein extracts from human OSCC cell lines. (C and D) Representative images of immunofluorescence for Scribble (red) with E-cadherin and Lgl1

(legend continued on next page)

right). In addition, miRNA-199b-5p delivery significantly enhanced the expression of Scribble, Lgl1, and E-cadherin compared with that in the control group (Figures 6B–6D). Immunofluorescence results showed that miRNA-199b-5p strongly preserved the localization of Scribble in the cell-cell region in tumors compared with that in the control (Figure 6E), and the co-localization of Scribble and Lgl1 was tightly maintained (Figure 6F). The results of hAlu sequence analysis indicated that the expression of the hAlu sequence was significantly downregulated in the lung tissues of the miRNA-199b-5p-overexpressing group compared with the control group (Figure 6G). Additionally, hematoxylin and eosin (H&E) staining revealed that, in contrast to the Scribble knockdown experiment, there was a significant reduction in OSCC metastasis to the lungs in the group overexpressing miRNA-199b-5p compared with that in the control group (Figure 6H). Based on these findings, our results suggest that enhanced expression of Scribble in the cell-cell region, mediated indirectly by miRNA-199b-5p, effectively inhibits both the growth and metastasis of OSCC.

DISCUSSION

In general, the integrity of cell junctions is important for maintaining the cell-cell barrier and homeostasis, which are pathologically related, such as in cancer or inflammation.[38,39] These epithelia consist of tight junction proteins and AJs, including zonula occludens-1, proteinase-activated receptor 3, catenins, and cadherins, and disruption of these genes has an important effect on the progression of various carcinomas.[40,41] This loss of polarity and cell-cell adhesion can also lead to infiltration and metastasis of cancers of epithelial origin to adjacent tissues, leading to adverse effects on progression and prognosis.[42] There have been reports that the hypoxic environment has damaged cell polarity in human breast epithelial cells, followed by tumor growth factor-beta-mediated destruction in the Madin-Darby canine kidney (MDCK) cell line,[43] but studies on how hypoxia is associated with cell polarity in relation to cell-cell contact in cancer are insufficient, especially in OSCC. In a previous study, we have shown that hypoxic conditions modulate the localization and expression of the tight junction and proteinase activator recptor3 (Par3), which may play an important role in the progression and metastasis of OSCC.[34] Unlike tight junction proteins, the expression and localization of AJs in our data was still ambiguous. To further investigate the role of basolateral proteins, this study aimed to investigate the effects of hypoxia on ABP in OSCC.

The most commonly linked pathway to metastasis is well known for the EMT, which is strongly associated with hypoxia in epithelial cells.[22,44] EMT is a process in which the epithelial cells of a tumor change into mesenchymal cells and is associated with tumor progression, invasion, and metastasis.[45,46] Recent studies have shown that EMT in various tumors does not have one characteristic but rather mixed characteristics of epithelial and mesenchymal cells.[47,48] These hybrid epithelial/mesenchymal (hybrid E/M) cells co-express epithelium (E-cadherin1 and epithelial cell adhesion molecule) and mesenchymal (vimentin, snail family transcriptional repressor 2, zinc finger E-Box binding homeobox 1) markers and form circulating tumor cell clusters that can move collectively and affect more lethal cell metastases in various cancers.[49–52] Therefore, at this hybrid E/M stage, called partial EMT (pEMT), ABPs and adherens proteins are reduced, resulting in increased mobility.[53] In OSCC, epithelial and pEMT markers are simultaneously overexpressed in tumor tissues, while mesenchymal markers are underexpressed.[54] Notably, the expression of these conflicting markers is dependent on the location of the primary tumor: epithelial markers are located in the center of the primary tumor, and pEMT markers are located at the leading edge of the primary tumor.[55] In our previous study, we demonstrated that HSC-2 cell lines are OSCC cells with characteristics of pEMT, expressing E-cadherin and exhibiting a mesenchymal phenotype.[34] Therefore, in this study we analyzed the effect of hypoxia and miRNA-199b-5p on ABP via Scribble in both the HSC-2 (pEMT) and SCC-9 (epithelial like) cell lines.

As miRNAs have been studied as potential therapeutic targets, Zhao et al. demonstrated that HRM can control angiogenesis and cancer against HIF-1/vascular endothelial growth factor,[56] and Winther et al. demonstrated the possibility that miR-210-mediated HRM in ESCC may be a potential marker of prognosis and treatment.[57] Studies have shown that miR-198, miR-487-3p, and miR-199a inhibit tumor growth, migration, and invasion[58–60]; however, studies on the effect of HRM on the regulation of cell formation and how they may be related are not yet sufficient. miRNAs have secondary and tertiary effects through direct inhibition or indirect targeting of mRNA targets.[61,62] Therefore, the target mRNA for miRNA should be supported by both experimental and bioinformatics evidence. After confirming that HIF-1α and miR-199b-5p showed significantly higher targeting using the miRDB, Targetscan, and miRTarBase databases (Figure S1A), we investigated the activity of HIF-1α in OSCC cells in the presence or absence of miR-199b-5p treatment. In contrast to the increase in HIF-1α expression by hypoxia, the results showed decreased luciferase activity by miR-199b-5p and supported that miR-199b-5p binds directly to HIF-1α. Furthermore, we confirmed that miR-199b-5p strengthened ABP in OSCC, and cell mobility and cell proliferation were suppressed in a Scribble-dependent manner. This was also confirmed in mice, where miR-199b-5p increased the RNA expression of Scribble/Lgl1/E-cadherin, affecting the reduction of tumor size and metastasis. Our overall results suggest that miRNA-199b-5p, which is targeted by HIF-1α, may indirectly regulate Scribble/Lgl1/E-cadherin expression and may be a potential effector of tumor growth and prognosis in OSCC.

(green) transfected by miR-199b in SCC-9 cell line. The z stacks were analyzed in three confocal slices. Original histology magnification, ×60. Scale bar, 20 μm. (E and F) Representative images (left) and numbers (right) of migrated and invaded cells transfected by miR-199b in SCC-9 and HSC-2 cell line. Original histology magnification, ×20. Scale bar, 100 μm. (G and H) Representative images (left) and numbers (right) of EdU-positive cells (green) for proliferation analysis transfected by miR-199b. The nuclei were stained with DAPI (blue). Original histology magnification, ×20. Scale bar, 20 μm. Statistical significance was assessed by Student's t test. $^{***}p < 0.001$, $^{**}p < 0.01$, $^{*}p < 0.05$.

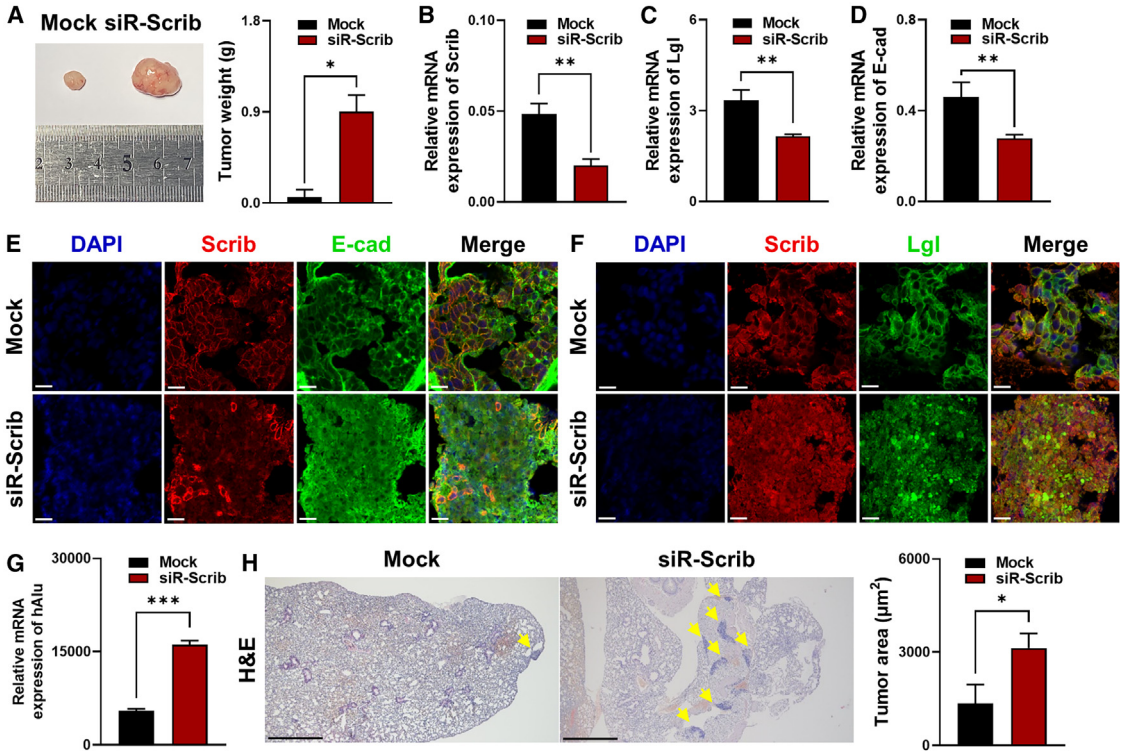

Figure 5. Scribble induces cell proliferation and metastasis *in vitro*

(A) Representative image (left) and tumor weight (right) by inhibiting Scribble from BALB/c nude mice xenograft injection ($n = 5$). (B, C, and D) Relative mRNA expression level of Scribble, Lgl and E-cadherin using real-time PCR from RNA extracts of mice xenograft tumor by inhibiting Scribble. (E and F) Representative images of immunofluorescence for Scribble (red) with E-cadherin and Lgl1 (green) by inhibiting Scribble from frozen sections of mice tumors. The nuclei were stained with DAPI (blue). Original histology magnification, ×60. Scale bar, 10 μm. (G) Relative mRNA expression level of hAlu using real-time PCR from RNA extracts of mice xenograft tumors. (H) Representative images (left) and graph of tumor area (right) of hematoxylin and eosin histologic staining in the mice lung from tail vein injection by inhibiting Scribble in OSCC cells. Statistical significance was assessed by Student's t test. ***$p < 0.001$, **$p < 0.01$, *$p < 0.05$.

However, our current study also has several limitations. First, Dlg1, which typically localizes at cell-cell contacts and regulates cell polarity with Scribble, behaved differently in our observations. Second, there is a lack of research on the direct molecular mechanisms by which miRNA-199b-5p alters ABP. Third, although we supplemented our study with epithelial-like HSC-4 cell lines, the bias of our cell polarity and *in vivo* results toward SCC-9 cell lines is a limitation. This must be investigated and resolved by improving the analytical techniques in future studies.

In summary, our study shows that the Scribble stream is important for maintaining ABP by forming a cell-cell barrier and modulating the progression and metastasis of OSCC via Lgl1. In particular, this stream suggests that it maybe indirectly regulated by miR-199b-5p, which directly targets HIF-1α (Figure 7). Our study offers new insights for therapeutic and diagnostic research by examining junction morphology in relation to Scribble expression. It also lays a strong foundation for developing new therapies targeting miRNA expression to reduce OSCC development and metastasis, thereby enhancing the potential of using miRNA and polarity proteins as a diagnostic marker for improving the prognosis of OSCC patients in the future.

MATERIALS AND METHODS

Clinical specimen and human tissue samples

A total of 33 paired OSCC patient tissues (tumor and adjacent normal tissue) were obtained in accordance with the ethical procedures of the Gangneung-Wonju National University Dental Hospital, Gangneung, Korea, and all patients agreed to participate. OSCC tissues were histopathologically diagnosed by a pathologist. Our study was approved by the Committee for Ethical Review of Research at Gangneung-Wonju National University (institutional review board no. GWNUIRB-2020-26-1). All tissues were prepared in advance from paraffin tissue sections after surgery, and the tissues were scored as described previously after immunohistochemical staining[34] (Table S1). To identify differentially expressed genes in OSCC samples (GSE 37991) compared with non-cancerous samples, we applied DEseq2 (https://www.bioconductor.org/). Differentially expressed genes were filtered according to the criteria of adj.$p < 0.001$ and $|\log2\text{ (fold-change)}| > 1$.

Cell culture and transfection

SCC-9, HSC-2, and HSC-4 cell lines were obtained from the American Type Culture Collection and the Japanese Collection

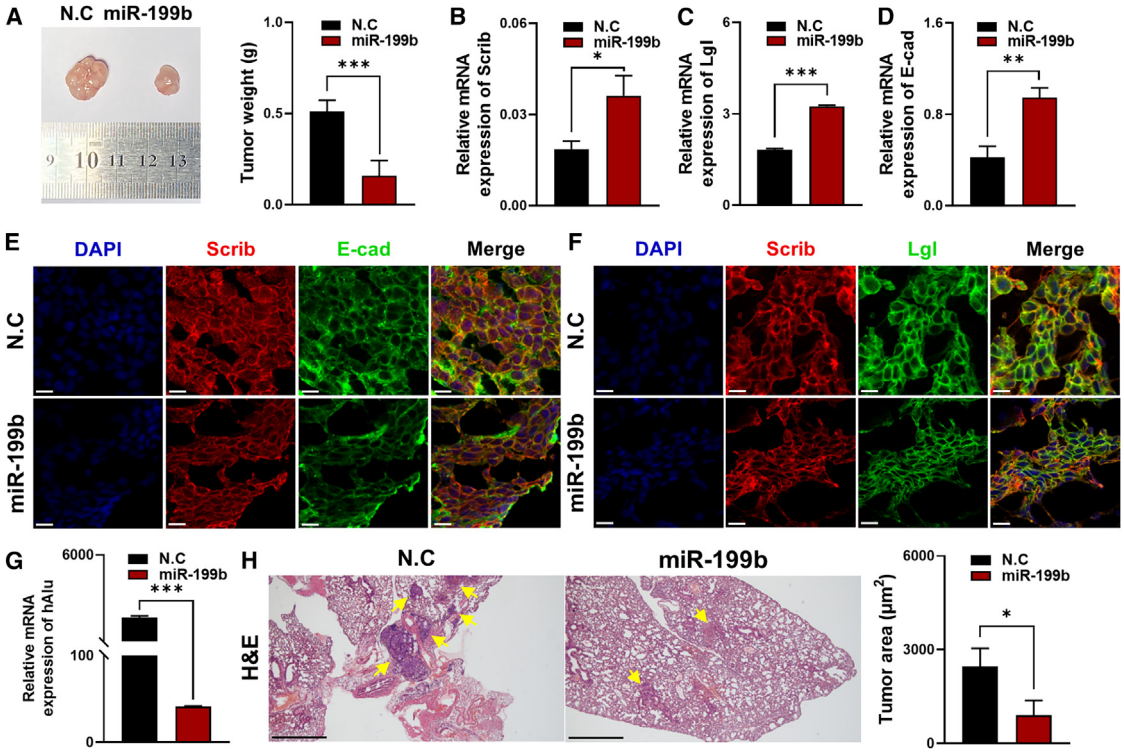

Figure 6. miR-199b-5p reduces cell proliferation and metastasis *in vitro*

(A) Representative image (left) and tumor weight (right) by miR-199b from BALB/c nude mice xenograft injection ($n = 5$). (B, C, and D) Relative mRNA expression level of Scribble, Lgl1 and E-cadherin using real-time PCR from RNA extracts of mice xenograft tumor by inhibiting Scribble. (E and F) Representative images of immunofluorescence for Scribble (red) with E-cadherin and Lgl1 (green) by miR-199b from frozen sections of mice tumors. The nuclei were stained with DAPI (blue). Original histology magnification, ×60. Scale bar, 10 μm. (G) Relative mRNA expression level of hAlu using real-time PCR from RNA extracts of mice xenograft tumor by inhibiting Scribble. (H) Representative images (left) and graph of the tumor area (right) of hematoxylin and eosin histologic staining in the mice lung from tail vein injection by miR-199b in OSCC cells. Statistical significance was assessed by Student's t test. ***$p < 0.001$, **$p < 0.01$, *$p < 0.05$.

of Research Bioresources Cell Bank. The SCC-9 cell line was cultured in Dulbecco's modified Eagle's medium/F-12 (Gibco, Ref# 11330-032) with 10% fetal bovine serum (FBS) and supplemented with 1% penicillin/streptomycin. HSC-2 cells were cultured in high-glucose Dulbecco's modified Eagle's medium (Invitrogen, Ref# SH30022.01) with 10% FBS and supplemented with 1% penicillin/streptomycin. The OSCC cell lines were incubated at 37°C in a humidified atmosphere of 5% CO_2 under normoxic conditions or 5% CO_2 and 1.5% O_2 balanced with N_2 under hypoxic conditions in a HeracellTM 150i CO_2 incubator (Thermo Fisher Scientific).

For siRNA-Scribble transfection, SCC-9 and HSC-2 cell lines were transfected with siRNA-negative control (Bioneer, Ref# SN-1001) or 50 nM siRNA-Scribble (Bioneer, custom ordered) for 6 h using Lipofectamine 2000 (Invitrogen, Ref# 11668-019) and Opti-MEM (Gibco, Ref# 31985-070) according to the manufacturer's instructions. For miRNA-199b-5p transfection, SCC-9 and HSC-2 cell lines were transfected with miRNA-negative control (Bioneer, Ref# SMC-2001) and 100 nM has-miR-199b-5p (Bioneer custom ordered) using Lipofectamine RNAiMAX Transfection Reagent (Invitrogen, Ref# 13778030) and Opti-MEM (Gibco) for 6 h according to manufacturer's instructions. Following transfection, all cells were incubated at 37°C in a humidified atmosphere of 5% CO_2 for 24 h. The sequences of the siRNA and miRNA mimic used were as follows: siRNA-Scribble: 5′-GUG AUG UUU GUA CAA CCA A-3′ and has-miR-199b-5p mimic: 5′-CCC AGU GUU UAG ACU AUC UGU UC-3′.

Immunoblot assays

Total protein was extracted from SCC-9 and HSC-2 cell lines or OSCC tissues using 1× RIPA buffer (Sigma-Aldrich, Ref# R0278) containing a protease inhibitor cocktail (Roche Diagnostics, Ref# 11697498001). Samples were incubated at 95 °C with 1× sodium dodecyl sulfate loading buffer for 5 min and loaded onto 8%–10% of sodium dodecyl sulfate-polyacrylamide gels and transferred onto nitrocellulose membranes. The membranes were blocked with 5% bovine serum albumin in phosphate-buffered saline with Tween (PBS-T) for 30 min at room temperature and incubated with primary antibodies at 4°C overnight. The membranes were probed with primary and secondary antibodies (Table S2). Protein expression was detected using a FUSION

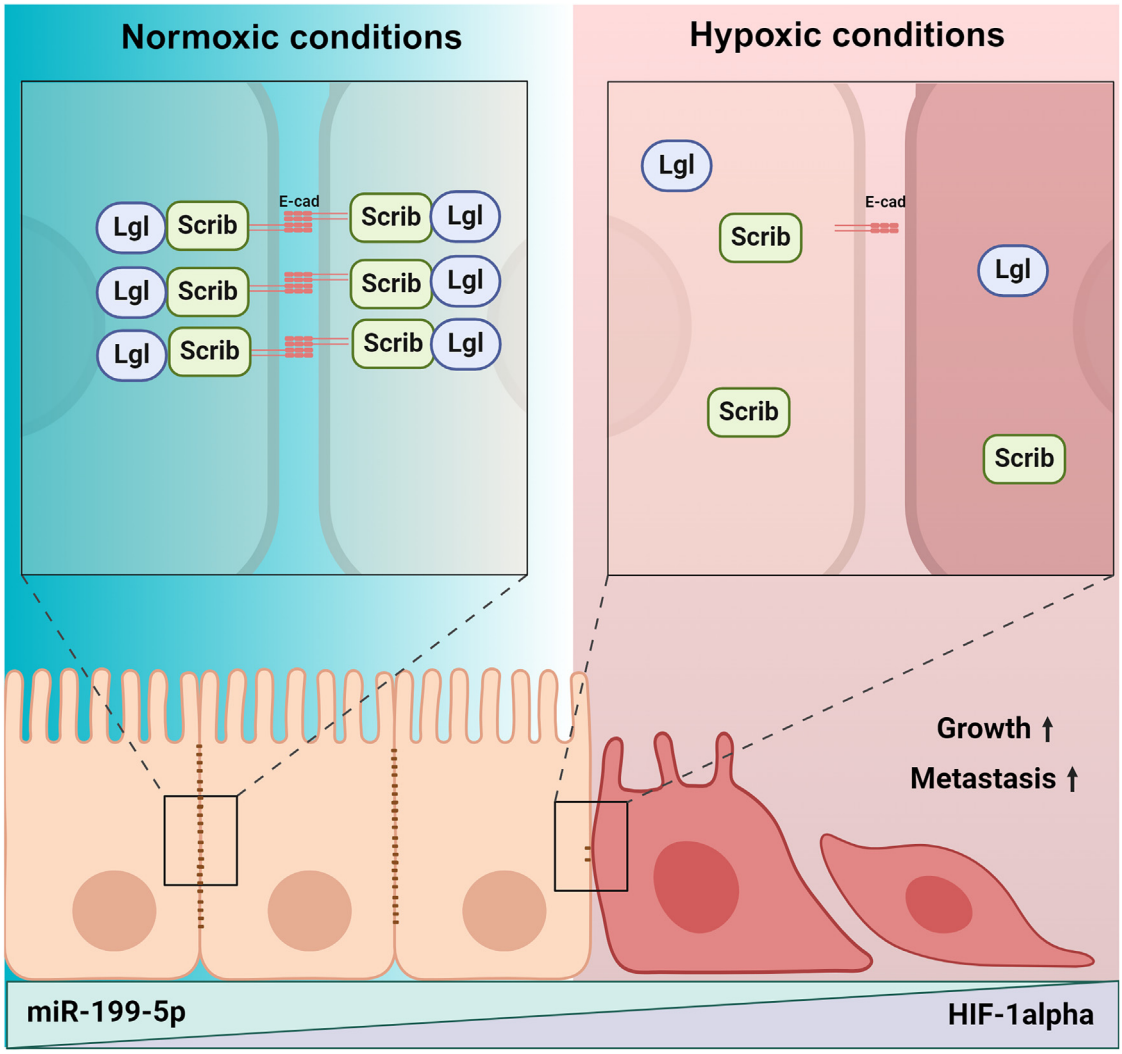

Figure 7. A schematic model miRNA-199b-5p and HIF-1α induced by hypoxic conditions in OSCC

Solo S imaging system (Vilber, Eberhardzell) with a chemiluminescent reagent (Millipore, Ref# wbluf0100).

Co-immunoprecipitation assays

After the indicated transfection, cell lysates were resuspended with Pierce IP Lysis Buffer (Thermo Fisher Scientific, Ref# 87787) supplemented with a protease inhibitor cocktail (Roche Diagnostics) and incubated 20 min on ice. The debris was cleared through centrifugation at 13,000 × *g* for 10 min. The lysates were incubated with Protein A Sepharose (Cytiva, Ref# 17078001) for 1 h at 4°C with rotation. Aliquots of lysates (1 mg) were incubated with 4 μg/mL of mouse anti-Scribble (1:1,000, Novus Biologicals, Ref #NBP2-29765) overnight at 4°C. The samples were washed with immunoprecipitation lysis buffer thrice for 5 min at 4°C with rotation. Immunoprecipitates were subjected to immunoblotting with rabbit anti-LLGL1 antibody (1:1,000, Abcam, Ref# ab183021).

Transwell migration and invasion assays

For the migration assay, each of the SCC-9 cells (4×10^4) or HSC-2 cells (8×10^3) were seeded in 24-well cell culture plates with 8.0-μm-pore Transwell inserts (Corning Inc., Ref# 353097). For the invasion assay, each of the SCC-9 cells (4×10^4) and HSC-2 cells (1×10^4) were seeded in BioCoat Matrigel Invasion Chambers with 8.0-μm-pore Transwell inserts (Corning Inc., Ref# 354480).Cells were transfected with siRNA-Scribble or miRNA-199b-5p, as described above. For chemoattraction, the lower chamber was filled with medium containing 10% FBS, whereas the upper chamber was not filled with FBS for 48 h. Transwell inserts were fixed with methanol for 20 min and stained with Mayer's hematoxylin histological staining reagent (Dako, Ref# S3309) at room temperature for 20 min. After removing the staining reagent, the inserts were mounted with a Mounting Medium (Dako, Ref# S3023) and observed under an inverted

microscope (Olympus, BX53). The number of migrated and invaded cells was captured in seven randomly selected fields and counted using the ImageJ software (National Institutes of Health).

EdU cell proliferation assay

For the EdU assay, Click-iT Plus EdU Alexa Fluor 488 Flow Cytometry Assay Kit (Abcam, Ref# C10337) was used according to the manufacturer's instructions. Briefly, each of the SCC-9 cells (2×10^5) and HSC-2 cells (2×10^5) were cultured and transfected with siRNA-Scribble or miRNA-199b-5p on coverslips, and then the cells were incubated with 10 μM EdU at 37°C in a humidified atmosphere of 5% CO_2 for 2 h. Coverslips were fixed with 4% paraformaldehyde for 20 min and permeabilized with 0.5% Triton X-100 for 20 min at room temperature. The coverslips were incubated with the click reaction cocktail provided in the Click-iT kit in the dark at room temperature for 40 min and mounted using Fluoroshield Mounting Medium with DAPI (Abcam). Seven images were captured randomly using a fluorescence microscope (Olympus), and EdU-positive cells were counted using ImageJ software.

Cloning of the vector construct

The target genes of human miR-199b-5p were predicted through bioinformatic analysis using the online database http://targetscan.org. Genomic DNA was isolated from HSC-2 cells, and its concentration and purity were examined using a Nanodrop (Thermo Fisher Scientific). The 3′-untranslated region (UTR) of human *HIF1A*, containing a binding site for human miR-199b-5p, was amplified using PCR using human genomic DNA. The PCR product was purified using an AccuPrep PCR Purification Kit (Bioneer, Ref# K-3037), digested with the restriction enzymes *XhoI* and *NotI*, and cloned into the psiCHECK-2 vector (Promega). The vector construct with 3′-UTR of HIF1-α was transformed into *Escherichia coli,* and then plasmid DNA was extracted from well-transformed, ampicillin-resistant *E. coli*, using an AccuPrep Plasmid Mini Extraction Kit (Bioneer, Ref# K-3030). The sequences of the miR-199b-5p-binding site of the 3′-UTR of HIF1-α were confirmed using sequencing analysis (Macrogen). The primer sequences used for vector construction are listed in Table S3. A commercially available pMirTarget vector cloned with 3′-UTR of HIF1A transcript was purchased (OriGene).

Luciferase reporter assay

SCC-9 cells (6×10^3) and HSC-2 cells (5×10^3) were cultured in 96-well plates and incubated in culture media without antibiotics at 37°C for 24 h. Both OSCC cell lines were transfected with a mixture of pMirTarget or psiCHECK-2 vector constructs and either an miR-199b-5p mimic (20 or 50 nM; AccuTarget human miR-199b-5p mimic; Bioneer) or the same concentration of scrambled miRNA (miRNA mimic negative control 1; Bioneer) as a negative control using Lipofectamine 3000 (Invitrogen, Ref# L3000001). After 30 h, the cells were harvested and tested using a Dual-Glo Luciferase Assay System (Promega, Ref# E2920) according to the manufacturer's protocol. All the Renilla luciferase activity data were normalized to firefly luciferase activity.

In vivo tumor growth and metastasis

Animal experiments were approved by the Ethics Committee on Animal Experiments of Gangneung-Wonju National University (Permit number: GWNU-2020-36-1) and were performed in accordance with the relevant guidelines. For the xenograft, SCC-9 cells (2×10^6) in 100 μL of Dulbecco's PBS (DPBS) were injected subcutaneously into 5-week-old male BALB/c nude mice. The tumor size was monitored every 3 days until a volume of approximately 1.5 mm^3 by calculating 0.52 × width2 × length.[63,64] Then, the mice were euthanized, and the tumors were quickly frozen in liquid nitrogen for mRNA expression analysis or storage at −80°C with Tissue-Tek O.C.T Compound (SAKURA Finetek, Ref# 4583) for frozen section immunofluorescence.

For metastasis, SCC-9 cells (2×10^6) in 100 μL of DPBS were injected into 8-week-old male BALB/c nude mice. After 5 weeks, the mice were euthanized, and the lungs were formalin-fixed for H&E staining. Parts of the lungs were quickly frozen in liquid nitrogen and analyzed for hAlu mRNA expression.

Real-time PCR

Total RNA was isolated from xenograft tumors or lungs of BALB/c nude mice using TRIzol reagent (Invitrogen, Ref# 15596026). cDNA (500 ng) was synthesized using AccuPower RocketScript Cycle RT PreMix (Bioneer, Ref# K-2101) according to the manufacturer's instructions. qPCR was analyzed using the CFX96 Touch Real-Time PCR system (Bio-Rad) with SYBR AccuPower 2X GreenStar qPCR Master Mix (Bioneer, Ref# K-6251), and denaturation was performed at 95°C for 15 s, followed by amplification at 62°C for 1 min in 40 cycles. The glyceraldehyde-3-phosphate dehydrogenase (GAPDH) was used to normalize mRNA expression level, and relative target gene expression levels were calculated using the 2–ΔΔCT method. The sequences of the gene-specific primers were as follows: human Scribble forward 5′-AAA CAG GGC TGA AGA GGA AG-3′ and reverse 5′-CAG GCT CTA TCA GCA GGT TAT T-3′; Lgl1 forward 5′-CCT CTT CCA GAC AGA CTG TGA G-3′ and reverse 5′-AGA GCA ACC TTC TGC ACG CCA A -3′; E-cadherin forward 5′-GCC TCC TGA AAA GAG AGT GGA AG-3′ and reverse 5′-TGG CAG TGT CTC TCC AAA TCC G-3′; GAPDH forward 5′-CAA AGT TGT CAT GGA TGA CC-3′ and reverse 5′-CCA TGG AGA AGG CTG GGG-3′; hsa-miR-199b-5p forward 5′-CCA GTG TTT AGA CTA TCT G-3′ and reverse 5′-GAA CAT GTC TGC GTA TCT C-3′; U6 forward 5′-CTC GCT TCG GCA GCA CAT-3′ and reverse 5′-TTT GCG TGT CAT CCT TGC G-3′; human-Alu forward 5′- CAT GGT GAA ACC CCG TCT CTA-3′ and reverse 5′-GCC TCA GCC TCC CGA GTA G-3′.

Immunofluorescence

For *in vitro* experiments, SCC-9 cells (2×10^5) were cultured under the aforementioned conditions. In the case of *in vivo* experiments, 7-μm cryosections of tumor tissue were obtained after the xenograft model and then fixed with 4% paraformaldehyde for 20 min. After being permeabilized with 0.5% Triton X-100 for 20 min at room temperature, samples were washed with DPBS. Samples were incubated for 1 h and probed with primary antibodies (Table S2) at room

temperature. After washing three times with DPBS, the coverslips were incubated with secondary antibodies labeled with Alexa Fluor 488 or Alexa Fluor 568 (Invitrogen, Ref# A32723) for an hour at room temperature. After washing with DPBS, the samples were mounted using Fluoroshield Mounting Medium with DAPI (Abcam). All images were acquired as a series of z stack confocal images using a STELLARIS 5 confocal microscope (×63 oil objective lens, Leica Microsystems) and described with stack/maximum projection using LAS X Science Microscope Software (Leica Microsystems).

Histological analysis

Tissue samples obtained from patients with OSCC or *in vivo* experiments were subjected to IHC analysis and evaluated by two pathologists. The tissues were sliced into 4-μm paraffin sections. The slides were deparaffinized, rehydrated with xylene, and then rehydrated in serial dilutions of ethanol. After incubation with 3% H_2O_2 for 30 min, the slides were incubated in antigen retrieval solution (sodium sulfate buffer, pH 6.0). To block the nonspecific binding, slides were incubated with 4% bovine serum albumin, probed with primary antibodies detailed in Table S2, and applied at 4°C overnight. After a brief wash with PBS, the slides were incubated with biotinylated goat anti-rabbit IgG (Cell Signaling Technology, Ref# 7074) for 1 h. Staining was developed using 3,3′-diaminobenzidine (Abcam, Ref# 3236466), followed by H&E counterstaining. After dehydration with serial dilutions of ethanol, the slides were mounted using Canada balsam (DAEJUNG, Ref# 2525–4425). The images were captured using an inverted microscope with a DP74 camera (BX53; Olympus). To quantify lung metastasis of OSCC, lung sections were stained with H&E and quantified using the Measure Plugin of Cellsens software (Olympus).

Statistical analysis

Each experiment was performed in triplicate, and all data are presented as the mean ± standard error of the mean. Statistical differences were analyzed using two-tailed unpaired Student's t tests. Correlations between clinicopathological parameters and tumor IHC staining scores were analyzed using the Fisher's exact test. Statistical analyses were performed using SPSS software (version 20.0; SPSS Inc.). Statistical significance was set at $p < 0.05$. All experiments were performed at least in triplicate.

DATA AND CODE AVAILABILITY

The datasets used and analyzed during the present study are available from the corresponding author on reasonable request.

ACKNOWLEDGMENTS

This study was supported by the Basic Science Research Program through a National Research Foundation of Korea grant funded by the Korean Government (MSIT) (2020R1C1C1004007) and a National Research Foundation of Korea (NRF) grant funded by the Korean Government (MSIT) (RS-2023-00275944). No disclosures have been reported by the other authors.

AUTHOR CONTRIBUTIONS

Conceptualization: S.H.K. and J.H.C.; Writing - Original Draft: S.H.K.; Writing Review and Editing: S.H.K., J.H.C., S.Y.P., Y.J.K., J.E.H; Experimentation: S.H.K., J.H.C., S.Y.P., Y.J.K., J.E.H; Visualization: S.H.K.; Supervision: J.H.C.

DECLARATION OF INTERESTS

The authors declare no competing interests.

SUPPLEMENTAL INFORMATION

Supplemental information can be found online at https://doi.org/10.1016/j.omtn.2024.102363.

REFERENCES

1. Bouvard, V., Nethan, S.T., Singh, D., Warnakulasuriya, S., Mehrotra, R., Chaturvedi, A.K., Chen, T.H.H., Ayo-Yusuf, O.A., Gupta, P.C., Kerr, A.R., et al. (2022). IARC Perspective on Oral Cancer Prevention. N. Engl. J. Med. *387*, 1999–2005. https://doi.org/10.1056/NEJMsr2210097.

2. Diseases, G.B.D., and Injuries, C. (2020). Global burden of 369 diseases and injuries in 204 countries and territories, 1990-2019: a systematic analysis for the Global Burden of Disease Study 2019. Lancet *396*, 1204–1222. https://doi.org/10.1016/S0140-6736(20)30925-9.

3. Xie, L., and Shang, Z. (2022). Burden of oral cancer in Asia from 1990 to 2019: Estimates from the Global Burden of Disease 2019 study. PLoS One *17*, e0265950. https://doi.org/10.1371/journal.pone.0265950.

4. Bray, F., Ferlay, J., Soerjomataram, I., Siegel, R.L., Torre, L.A., and Jemal, A. (2018). Global cancer statistics 2018: GLOBOCAN estimates of incidence and mortality worldwide for 36 cancers in 185 countries. CA A Cancer J. Clin. *68*, 394–424. https://doi.org/10.3322/caac.21492.

5. Tomioka, H., Yamagata, Y., Oikawa, Y., Ohsako, T., Kugimoto, T., Kuroshima, T., Hirai, H., Shimamoto, H., and Harada, H. (2021). Risk factors for distant metastasis in locoregionally controlled oral squamous cell carcinoma: a retrospective study. Sci. Rep. *11*, 5213. https://doi.org/10.1038/s41598-021-84704-w.

6. Biyani, C.S., Campain, N., Moore, M., Gobezie, A., Teferi, G.T., and MacDonagh, R.; BAUS Urolink committee (2019). Urolink supporting the development of urological services in Hawassa, Ethiopia. BJU Int. *123*, 917–920. https://doi.org/10.1111/bju.14670.

7. Heikenwalder, M., and Lorentzen, A. (2019). The role of polarisation of circulating tumour cells in cancer metastasis. Cell. Mol. Life Sci. *76*, 3765–3781. https://doi.org/10.1007/s00018-019-03169-3.

8. Chaffer, C.L., San Juan, B.P., Lim, E., and Weinberg, R.A. (2016). EMT, cell plasticity and metastasis. Cancer Metastasis Rev. *35*, 645–654. https://doi.org/10.1007/s10555-016-9648-7.

9. Pandya, P., Orgaz, J.L., and Sanz-Moreno, V. (2017). Modes of invasion during tumour dissemination. Mol. Oncol. *11*, 5–27. https://doi.org/10.1002/1878-0261.12019.

10. Celia-Terrassa, T., and Kang, Y. (2016). Distinctive properties of metastasis-initiating cells. Genes Dev. *30*, 892–908. https://doi.org/10.1101/gad.277681.116.

11. Cai, J., Qiao, B., Gao, N., Lin, N., and He, W. (2019). Oral squamous cell carcinoma-derived exosomes promote M2 subtype macrophage polarization mediated by exosome-enclosed miR-29a-3p. Am. J. Physiol. Cell Physiol. *316*, C731–C740. https://doi.org/10.1152/ajpcell.00366.2018.

12. Gandalovicova, A., Vomastek, T., Rosel, D., and Brabek, J. (2016). Cell polarity signaling in the plasticity of cancer cell invasiveness. Oncotarget *7*, 25022–25049. https://doi.org/10.18632/oncotarget.7214.

13. Schmidt, A., and Peifer, M. (2020). Scribble and Dlg organize a protection racket to ensure apical-basal polarity. Proc. Natl. Acad. Sci. USA *117*, 13188–13190. https://doi.org/10.1073/pnas.2007739117.

14. Shen, H., Huang, C., Wu, J., Li, J., Hu, T., Wang, Z., Zhang, H., Shao, Y., and Fu, Z. (2021). *SCRIB* Promotes Proliferation and Metastasis by Targeting Hippo/YAP Signalling in Colorectal Cancer. Front. Cell Dev. Biol. *9*, 656359. https://doi.org/10.3389/fcell.2021.656359.

15. Stephens, R., Lim, K., Portela, M., Kvansakul, M., Humbert, P.O., and Richardson, H.E. (2018). The Scribble Cell Polarity Module in the Regulation of Cell Signaling in Tissue Development and Tumorigenesis. J. Mol. Biol. *430*, 3585–3612. https://doi.org/10.1016/j.jmb.2018.01.011.

16. Vaira, V., Faversani, A., Dohi, T., Maggioni, M., Nosotti, M., Tosi, D., Altieri, D.C., and Bosari, S. (2011). Aberrant overexpression of the cell polarity module scribble

in human cancer. Am. J. Pathol. *178*, 2478–2483. https://doi.org/10.1016/j.ajpath.2011.02.028.

17. Sakakibara, J., Sakakibara, M., Shiina, N., Fujimori, T., Okubo, Y., Fujisaki, K., Nagashima, T., Sangai, T., Nakatani, Y., and Miyazaki, M. (2017). Expression of cell polarity protein scribble differently affects prognosis in primary tumor and lymph node metastasis of breast cancer patients. Breast Cancer *24*, 393–399. https://doi.org/10.1007/s12282-016-0715-2.

18. Edamana, S., Login, F.H., Riishede, A., Dam, V.S., Tramm, T., and Nejsum, L.N. (2023). The cell polarity protein Scribble is downregulated by the water channel aquaporin-5 in breast cancer cells. Am. J. Physiol. Cell Physiol. *324*, C307–C319. https://doi.org/10.1152/ajpcell.00311.2022.

19. Wang, N., Song, L., Xu, Y., Zhang, L., Wu, Y., Guo, J., Ji, W., Li, L., Zhao, J., Zhang, X., and Zhan, L. (2019). Loss of Scribble confers cisplatin resistance during NSCLC chemotherapy via Nox2/ROS and Nrf2/PD-L1 signaling. EBioMedicine *47*, 65–77. https://doi.org/10.1016/j.ebiom.2019.08.057.

20. Simsek, H., and Klotzsch, E. (2022). The solid tumor microenvironment-Breaking the barrier for T cells: How the solid tumor microenvironment influences T cells: How the solid tumor microenvironment influences T cells. Bioessays *44*, e2100285. https://doi.org/10.1002/bies.202100285.

21. Nakamura, N., Shi, X., Darabi, R., and Li, Y. (2021). Hypoxia in Cell Reprogramming and the Epigenetic Regulations. Front. Cell Dev. Biol. *9*, 609984. https://doi.org/10.3389/fcell.2021.609984.

22. Tam, S.Y., Wu, V.W.C., and Law, H.K.W. (2020). Hypoxia-Induced Epithelial-Mesenchymal Transition in Cancers: HIF-1α and Beyond. Front. Oncol. *10*, 486. https://doi.org/10.3389/fonc.2020.00486.

23. Zhao, Y., Xing, C., Deng, Y., Ye, C., and Peng, H. (2024). HIF-1α signaling: Essential roles in tumorigenesis and implications in targeted therapies. Genes Dis. *11*, 234–251. https://doi.org/10.1016/j.gendis.2023.02.039.

24. Lin, Y.T., and Wu, K.J. (2020). Epigenetic regulation of epithelial-mesenchymal transition: focusing on hypoxia and TGF-beta signaling. J. Biomed. Sci. *27*, 39. https://doi.org/10.1186/s12929-020-00632-3.

25. Sawai, S., Wong, P.F., and Ramasamy, T.S. (2022). Hypoxia-regulated microRNAs: the molecular drivers of tumor progression. Crit. Rev. Biochem. Mol. Biol. *57*, 351–376. https://doi.org/10.1080/10409238.2022.2088684.

26. Moriondo, G., Scioscia, G., Soccio, P., Tondo, P., De Pace, C.C., Sabato, R., Foschino Barbaro, M.P., and Lacedonia, D. (2022). Effect of Hypoxia-Induced Micro-RNAs Expression on Oncogenesis. Int. J. Mol. Sci. *23*, 6294. https://doi.org/10.3390/ijms23116294.

27. Silina, M.V., Dzhalilova, D.S., and Makarova, O.V. (2023). Role of MicroRNAs in Regulation of Cellular Response to Hypoxia. Biochemistry *88*, 741–757. https://doi.org/10.1134/S0006297923060032.

28. Hong, X., and Yu, J.J. (2019). MicroRNA-150 suppresses epithelial-mesenchymal transition, invasion, and metastasis in prostate cancer through the TRPM4-mediated beta-catenin signaling pathway. Am. J. Physiol. Cell Physiol. *316*, C463–C480. https://doi.org/10.1152/ajpcell.00142.2018.

29. Tung, C.H., Kuo, L.W., Huang, M.F., Wu, Y.Y., Tsai, Y.T., Wu, J.E., Hsu, K.F., Chen, Y.L., and Hong, T.M. (2020). MicroRNA-150-5p promotes cell motility by inhibiting c-Myb-mediated Slug suppression and is a prognostic biomarker for recurrent ovarian cancer. Oncogene *39*, 862–876. https://doi.org/10.1038/s41388-019-1025-x.

30. Lu, W., Zhang, H., Niu, Y., Wu, Y., Sun, W., Li, H., Kong, J., Ding, K., Shen, H.M., Wu, H., et al. (2017). Long non-coding RNA linc00673 regulated non-small cell lung cancer proliferation, migration, invasion and epithelial mesenchymal transition by sponging miR-150-5p. Mol. Cancer *16*, 118. https://doi.org/10.1186/s12943-017-0685-9.

31. Jin, H., Jin, X., Chai, W., Yin, Z., Li, Y., Dong, F., and Wang, W. (2019). Long non-coding RNA MIAT competitively binds miR-150-5p to regulate ZEB1 expression in osteosarcoma. Oncol. Lett. *17*, 1229–1236. https://doi.org/10.3892/ol.2018.9671.

32. Abedrabbo, M., Sloomy, S., Abu-Leil, R., Kfir-Cohen, E., and Ravid, S. (2023). Scribble, Lgl1, and myosin IIA interact with α-/β-catenin to maintain epithelial junction integrity. Cell Adhes. Migrat. *17*, 1–23. https://doi.org/10.1080/19336918.2023.2260645.

33. Bonello, T.T., Choi, W., and Peifer, M. (2019). Scribble and Discs-large direct initial assembly and positioning of adherens junctions during the establishment of apical-basal polarity. Development *146*, dev180976. https://doi.org/10.1242/dev.180976.

34. Kim, S., Park, S., Moon, E.H., Kim, G.J., and Choi, J. (2023). Hypoxia disrupt tight junctions and promote metastasis of oral squamous cell carcinoma via loss of par3. Cancer Cell Int. *23*, 79. https://doi.org/10.1186/s12935-023-02924-8.

35. Zhang, Y., Zhao, H.J., Xia, X.R., Diao, F.Y., Ma, X., Wang, J., Gao, L., Liu, J., Gao, C., Cui, Y.G., and Liu, J.Y. (2019). Hypoxia-induced and HIF1α-VEGF-mediated tight junction dysfunction in choriocarcinoma cells: Implications for preeclampsia. Clin. Chim. Acta *489*, 203–211. https://doi.org/10.1016/j.cca.2017.12.010.

36. Kim, S., Park, S., Oh, J.H., Lee, S.S., Lee, Y., and Choi, J. (2022). MicroRNA-18a regulates the metastatic properties of oral squamous cell carcinoma cells via HIF-1α expression. BMC Oral Health *22*, 378. https://doi.org/10.1186/s12903-022-02425-6.

37. Creane, M., Howard, L., O'Brien, T., and Coleman, C.M. (2017). Biodistribution and retention of locally administered human mesenchymal stromal cells: Quantitative polymerase chain reaction-based detection of human DNA in murine organs. Cytotherapy *19*, 384–394. https://doi.org/10.1016/j.jcyt.2016.12.003.

38. Marincola Smith, P., Choksi, Y.A., Markham, N.O., Hanna, D.N., Zi, J., Weaver, C.J., Hamaamen, J.A., Lewis, K.B., Yang, J., Liu, Q., et al. (2021). Colon epithelial cell TGFβ signaling modulates the expression of tight junction proteins and barrier function in mice. Am. J. Physiol. Gastrointest. Liver Physiol. *320*, G936–G957. https://doi.org/10.1152/ajpgi.00053.2021.

39. Kim, D.Y., Furuta, G.T., Nguyen, N., Inage, E., and Masterson, J.C. (2019). Epithelial Claudin Proteins and Their Role in Gastrointestinal Diseases. J. Pediatr. Gastroenterol. Nutr. *68*, 611–614. https://doi.org/10.1097/MPG.0000000000002301.

40. Bhat, A.A., Uppada, S., Achkar, I.W., Hashem, S., Yadav, S.K., Shanmugakonar, M., Al-Naemi, H.A., Haris, M., and Uddin, S. (2018). Tight Junction Proteins and Signaling Pathways in Cancer and Inflammation: A Functional Crosstalk. Front. Physiol. *9*, 1942. https://doi.org/10.3389/fphys.2018.01942.

41. Gonzalez-Mariscal, L., Miranda, J., Gallego-Gutierrez, H., Cano-Cortina, M., and Amaya, E. (2020). Relationship between apical junction proteins, gene expression and cancer. Biochim. Biophys. Acta Biomembr. *1862*, 183278. https://doi.org/10.1016/j.bbamem.2020.183278.

42. Coradini, D., Casarsa, C., and Oriana, S. (2011). Epithelial cell polarity and tumorigenesis: new perspectives for cancer detection and treatment. Acta Pharmacol. Sin. *32*, 552–564. https://doi.org/10.1038/aps.2011.20.

43. Raykhel, I., Moafi, F., Myllymaki, S.M., Greciano, P.G., Matlin, K.S., Moyano, J.V., Manninen, A., and Myllyharju, J. (2018). BAMBI is a novel HIF1-dependent modulator of TGFβ-mediated disruption of cell polarity during hypoxia. J. Cell Sci. *131*, jcs210906. https://doi.org/10.1242/jcs.210906.

44. Hapke, R.Y., and Haake, S.M. (2020). Hypoxia-induced epithelial to mesenchymal transition in cancer. Cancer Lett. *487*, 10–20. https://doi.org/10.1016/j.canlet.2020.05.012.

45. Pastushenko, I., and Blanpain, C. (2019). EMT Transition States during Tumor Progression and Metastasis. Trends Cell Biol. *29*, 212–226. https://doi.org/10.1016/j.tcb.2018.12.001.

46. Ribatti, D., Tamma, R., and Annese, T. (2020). Epithelial-Mesenchymal Transition in Cancer: A Historical Overview. Transl. Oncol. *13*, 100773. https://doi.org/10.1016/j.tranon.2020.100773.

47. George, J.T., Jolly, M.K., Xu, S., Somarelli, J.A., and Levine, H. (2017). Survival Outcomes in Cancer Patients Predicted by a Partial EMT Gene Expression Scoring Metric. Cancer Res. *77*, 6415–6428. https://doi.org/10.1158/0008-5472.CAN-16-3521.

48. Luond, F., Sugiyama, N., Bill, R., Bornes, L., Hager, C., Tang, F., Santacroce, N., Beisel, C., Ivanek, R., Burglin, T., et al. (2021). Distinct contributions of partial and full EMT to breast cancer malignancy. Dev. Cell *56*, 3203–3221.e3211. https://doi.org/10.1016/j.devcel.2021.11.006.

49. Jolly, M.K., Boareto, M., Huang, B., Jia, D., Lu, M., Ben-Jacob, E., Onuchic, J.N., and Levine, H. (2015). Implications of the Hybrid Epithelial/Mesenchymal Phenotype in Metastasis. Front. Oncol. *5*, 155. https://doi.org/10.3389/fonc.2015.00155.

50. Li, D., Xia, L., Huang, P., Wang, Z., Guo, Q., Huang, C., Leng, W., and Qin, S. (2023). Heterogeneity and plasticity of epithelial-mesenchymal transition (EMT) in cancer

metastasis: Focusing on partial EMT and regulatory mechanisms. Cell Prolif. *56*, e13423. https://doi.org/10.1111/cpr.13423.

51. Nieto, M.A., Huang, R.Y.J., Jackson, R.A., and Thiery, J.P. (2016). Emt: 2016. Cell *166*, 21–45. https://doi.org/10.1016/j.cell.2016.06.028.

52. Yu, M., Bardia, A., Wittner, B.S., Stott, S.L., Smas, M.E., Ting, D.T., Isakoff, S.J., Ciciliano, J.C., Wells, M.N., Shah, A.M., et al. (2013). Circulating breast tumor cells exhibit dynamic changes in epithelial and mesenchymal composition. Science *339*, 580–584. https://doi.org/10.1126/science.1228522.

53. Saliem, S.S., Bede, S.Y., Cooper, P.R., Abdulkareem, A.A., Milward, M.R., and Abdullah, B.H. (2022). Pathogenesis of periodontitis - A potential role for epithelial-mesenchymal transition. Jpn. Dent. Sci. Rev. *58*, 268–278. https://doi.org/10.1016/j.jdsr.2022.09.001.

54. Wangmo, C., Charoen, N., Jantharapattana, K., Dechaphunkul, A., and Thongsuksai, P. (2020). Epithelial-Mesenchymal Transition Predicts Survival in Oral Squamous Cell Carcinoma. Pathol. Oncol. Res. *26*, 1511–1518. https://doi.org/10.1007/s12253-019-00731-z.

55. Puram, S.V., Tirosh, I., Parikh, A.S., Patel, A.P., Yizhak, K., Gillespie, S., Rodman, C., Luo, C.L., Mroz, E.A., Emerick, K.S., et al. (2017). Single-Cell Transcriptomic Analysis of Primary and Metastatic Tumor Ecosystems in Head and Neck Cancer. Cell *171*, 1611–1624.e24. https://doi.org/10.1016/j.cell.2017.10.044.

56. Zhao, C., and Popel, A.S. (2015). Computational Model of MicroRNA Control of HIF-VEGF Pathway: Insights into the Pathophysiology of Ischemic Vascular Disease and Cancer. PLoS Comput. Biol. *11*, e1004612. https://doi.org/10.1371/journal.pcbi.1004612.

57. Winther, M., Alsner, J., Sørensen, B.S., Wittrup, C.F., Tramm, T., Baeksgaard, L., Hofland, K., Holtved, E., and Nordsmark, M. (2016). Hypoxia-regulated MicroRNAs in Gastroesophageal Cancer. Anticancer Res. *36*, 721–730.

58. Kang, Y., Zhang, Y., and Sun, Y. (2021). MicroRNA-198 suppresses tumour growth and metastasis in oral squamous cell carcinoma by targeting CDK4. Int. J. Oncol. *59*, 39. https://doi.org/10.3892/ijo.2021.5219.

59. Wang, L., Ge, S., and Zhou, F. (2021). MicroRNA-487a-3p inhibits the growth and invasiveness of oral squamous cell carcinoma by targeting PPM1A. Bioengineered *12*, 937–947. https://doi.org/10.1080/21655979.2021.1884396.

60. Wei, D., Wang, W., Shen, B., Zhou, Y., Yang, X., Lu, G., Yang, J., and Shao, Y. (2019). MicroRNA-199a-5p suppresses migration and invasion in oral squamous cell carcinoma through inhibiting the EMT-related transcription factor SOX4. Int. J. Mol. Med. *44*, 185–195. https://doi.org/10.3892/ijmm.2019.4174.

61. Garcia, D.M., Baek, D., Shin, C., Bell, G.W., Grimson, A., and Bartel, D.P. (2011). Weak seed-pairing stability and high target-site abundance decrease the proficiency of lsy-6 and other microRNAs. Nat. Struct. Mol. Biol. *18*, 1139–1146. https://doi.org/10.1038/nsmb.2115.

62. Matkovich, S.J., Hu, Y., Eschenbacher, W.H., Dorn, L.E., and Dorn, G.W., 2nd (2012). Direct and indirect involvement of microRNA-499 in clinical and experimental cardiomyopathy. Circ. Res. *111*, 521–531. https://doi.org/10.1161/CIRCRESAHA.112.265736.

63. Tian, C., Zhou, J., Li, X., Gao, Y., Wen, Q., Kang, X., Wang, N., Yao, Y., Jiang, J., Song, G., et al. (2023). Impaired histone inheritance promotes tumor progression. Nat. Commun. *14*, 3429. https://doi.org/10.1038/s41467-023-39185-y.

64. Strazza, M., Moore, E.K., Adam, K., Azoulay-Alfaguter, I., and Mor, A. (2022). Neutralization of the adaptor protein PAG by monoclonal antibody limits murine tumor growth. Mol. Ther. Methods Clin. Dev. *27*, 380–390. https://doi.org/10.1016/j.omtm.2022.10.012.